Geophysical Research Letters®

Key Points:

- Analyses of ground magnetometer data from substorms during northward Interplanetary Magnetic Field (IMF) show that substorms impact the NBZ dayside ionospheric currents
- During substorms under northward IMF conditions, lobe cells are unusually weak before onset and become more distinct after
- We suggest possible mechanisms by which magnetotail dynamics can influence dayside ionospheric currents

Supporting Information:

Supporting Information may be found in the online version of this article.

Correspondence to:

R. Elhawary,
reham.elhawary@uib.no

Author Contributions:

Conceptualization: R. Elhawary, K. M. Laundal, J. P. Reistad
Formal analysis: R. Elhawary
Investigation: R. Elhawary, A. Ohma
Methodology: R. Elhawary
Software: M. Madelaire
Supervision: K. M. Laundal, J. P. Reistad
Validation: R. Elhawary
Writing – original draft: R. Elhawary
Writing – review & editing: R. Elhawary, K. M. Laundal, J. P. Reistad, M. Madelaire, A. Ohma

Substorm Impact on Dayside Ionospheric Currents

R. Elhawary[1] , K. M. Laundal[1] , J. P. Reistad[1] , M. Madelaire[1] , and A. Ohma[1]

[1]Birkeland Centre for Space Science, Department for Physics and Technology, University of Bergen, Bergen, Norway

Abstract Ionospheric dayside dynamics is strongly controlled by the interaction between the Interplanetary Magnetic Field (IMF) and the Earth's magnetic field near the dayside magnetopause, while nightside ionospheric dynamics depends mainly on magnetotail activity. However, we know little about the influence of magnetotail activity on the dayside ionospheric dynamics. We investigate this by performing superposed epoch analyses of ground magnetic field data for substorms occurring during northward IMF. In such substorms, dayside reconnection is minimized, allowing us to separate the effects of the magnetotail activity on the dayside current system. We find that as nightside activity elevates, the dayside ionospheric current elevates. Our analyses indicate that the lobe cells are less distinct before onset than during non-substorm northward IMF conditions. They become more pronounced after onset, possibly due to magnetospheric reconfiguration or a remote effect of the nightside current. We discuss possible mechanisms that may explain our observations.

Plain Language Summary Aurora in the high latitude upper atmosphere is a major observable illustration of events occurring in the nightside of the Earth's magnetosphere called substorms. Substorms increase the electric current of the upper atmosphere at high latitudes. The increment lasts for tens of minutes before it decays. The impact of substorms on the dayside current system is not known. We study substorms during certain conditions, and we find that the dayside currents also tend to increase with substorms. We discuss potential explanations of that influence on the dayside. Our findings help us understand the origins of the dynamics of the upper atmosphere.

1. Introduction

The interaction between the Interplanetary Magnetic Field (IMF) and the terrestrial magnetic field through magnetic reconnection is the primary driver of magnetosphere dynamics. During southward IMF, the Dungey cycle explains the ionospheric convection pattern in terms of dayside magnetic reconnection between the IMF and Earth's magnetosphere near the dayside magnetopause. Dayside reconnection leads to the opening of magnetic field lines and the expansion of the polar cap. The opened field lines stretch toward the nightside magnetotail equatorial plane. Eventually, the built-up pressure triggers nightside reconnection, causing the contraction of the polar cap as open field lines close. This dynamic process is known as the Expanding/Contracting Polar Cap paradigm (ECPC) (Cowley & Lockwood, 1992).

Although empirical models such as the Average Magnetic field and Polar current System model (AMPS) (Laundal et al., 2018) and the Weimer electric potential model (Weimer, 2005) provide insights into ionospheric dynamics in terms of IMF, their ability to capture the less predictable factors controlling nightside reconnection is limited. Previous studies (Grocott et al., 2002, 2017; Provan et al., 2004) have shown that substorms can dominate over convection driven by dayside reconnection. Additionally, there is evidence that dayside dynamics can influence nightside ionospheric convection via wave propagation mechanisms (Snekvik et al., 2017). While the impact of substorms on the nightside current system is known, the influence of substorms on the dayside current system requires more investigation. In this study, our primary objective is to investigate the influence of substorms on dayside ionospheric currents.

Substorms are a critical process in which the magnetosphere releases magnetic flux by reconnection in the neutral sheet of the magnetotail (Milan et al., 2010). During substorms, especially during southward IMF, both dayside and nightside can be highly dynamic. In-situ measurements of the solar wind and IMF makes it possible to quantify the dayside reconnection rate (Milan et al., 2012), but there is no similar proxy for nightside reconnection. This makes differentiating between the contribution of nightside and dayside reconnection on ionospheric dynamics very challenging to achieve. However, during northward IMF, the dayside experiences a minimal opening of flux and is only affected by IMF in a localized region in the dayside polar cap, while the nightside can

undergo magnetotail reconnection during substorms. Therefore, our study focuses on understanding the influence of substorms on dayside ionospheric convection during northward IMF.

During northward IMF, an intense and localized current system is established in the dayside polar cap (Iijima, 1984; Laundal et al., 2018; Milan, 2015). This current is referred to as the northward-directed B_z (NBZ), or lobe cells, due to its relation to lobe reconnection. We use the two terms interchangeably for the rest of the paper. The NBZ current system consists of two cells; a positive, upward-directed current in the pre-noon sector and a negative, downward-directed current in the post-noon sector, located poleward of the dayside region-1 current. The strength of the lobe cells reflects the reverse dayside convection pattern modulated by ionospheric conductance (Reistad et al., 2019).

In this study, we present a statistical analysis of the ionospheric current during northward IMF substorms by examining ground magnetic field perturbations above 60° latitude. The analysis is based on three substorm lists. Only substorms preceded by 45 min and followed by 20 min of northward IMF are considered in order to isolate substorm-induced dayside activity. Using each list, we perform a superposed epoch analysis using a spherical harmonic (SH) representation of the magnetic field. In Section 2, we discuss substorm lists and data analysis in detail. In Section 3, our findings demonstrate a dayside ionospheric response to the substorm onset. In Section 4, we discuss possible explanations for the influence of nightside dynamics on the dayside ionospheric current.

2. Data and Method

To investigate the ionospheric currents in the dayside during substorms with northward IMF, we used three different substorm lists to ensure that observed trends are not a signature of a specific substorm list. (a) The first list, FL: uses global ultraviolet (UV) imaging to identify substorm onsets. This list consists of two lists provided through Frey et al. (2004) and Liou (2010). (b) NG: is based on the SuperMAG AL (SML) index, which is a ground-based magnetometer index as described in detail in previous works (Newell & Gjerloev, 2011) between years 1990 and 2019. (c) SOPHIE S75 is based on SuperMAG AL (SML) index and uses a different algorithm to identify the substorm phases and the substorm onsets compared to the NG list, as discussed in Forsyth et al. (2015), between years 1990 and 2019.

While it is well-known that substorms are more common under southward IMF conditions, we limit our investigation to northward IMF substorms (Lee, Choi, et al., 2010; Lee, Ohtani, & Lee, 2010; Miyashita et al., 2011; Peng et al., 2013). We obtained solar wind measurements with a 1-min resolution from the OMNI data set which is propagated to represent the solar wind and IMF conditions at the bow shock. The solar wind data is presented in Geocentric Solar Magnetic coordinates. We defined a northward IMF substorm using a 65-min interval of northward IMF from 45 min prior to substorm onset to 20 min after onset. We permitted no data gaps during this interval, but allowed at most a total of 5 min of deviation from northward IMF throughout the interval. We chose the northward IMF 45-min criterion prior to onset to account for uncertainties in the solar wind time shift and to allow for the system reconfiguration due to the northward IMF turning as discussed in Yu and Ridley (2009), while a sufficient number of substorms remain for statistical analysis.

We limited the NG and S75 substorm lists to include only those events that were detected first by a magnetometer on the nightside (i.e., with magnetic local time between 18 and 06). As a slight positive bias in IMF B_y was observed in the substorm lists defined using ground-based indices (Ohma et al., 2021), we imposed an additional constraint that required the absolute value of the IMF clock angle, $\theta_{ca} = \arctan2(B_y, B_z)$, to be <45° from 45 min before substorm onset until 20 min after onset, allowing for a deviation of 5 min and no data gaps. However, the requirements were relaxed for the FL list in order to have sufficient events for a superposed epoch analysis. We implemented $|\theta_{ca}| < 70°$ restriction to minimize the potential effects of closed field line reconnection, as previous studies suggested its occurrence on the dayside equatorward of the cusp at absolute clock angles greater than 70° (Freeman et al., 1993; Senior et al., 2002). The OMNI data set also provided the AL index, which we used as another criterion for the S75 list, with a minimum AL index less than −100 nT to avoid false identification of substorms. With these criteria, the NG list had 236 events, S75 had 164 events, and FL had 143 events.

Although we used a large time window (−45, 20) min to capture the ionospheric response to the northward turning, it is possible that the response could be delayed due to the associated reconfiguration time (e.g., Snekvik et al., 2017; Tenfjord et al., 2017). To distinguish between a delayed influence of the IMF turning and the impact of substorms on the dayside ionospheric current, we applied the same stable northward IMF criterion to a control

group (CG) of non-substorm events. Specifically, we randomly selected 7,000 reference minutes between 1996 and 2005 and applied the same northward IMF and clock angle criteria, resulting in a CG list of 384 events for analysis.

In this study, we analyzed ground magnetic field perturbations from the SuperMAG database to investigate ionospheric currents in the high-latitude ($\geq 60°$) northern hemisphere. We used 1-min resolution magnetometer data with the baseline subtracted provided through SuperMAG (Gjerloev, 2012) and converted the magnetic field perturbations to quasi-dipole coordinates following Laundal et al. (2016) which we used in the SH representation.

To study the ionospheric currents based on the ground observations of magnetic field perturbations, we used a mathematical representation called the equivalent horizontal ionospheric current (EHIC) as discussed in Madelaire et al. (2022). The EHIC is related to the equivalent current function Ψ through

$$\vec{j}_{eq} = \hat{r} \times \nabla \Psi \tag{1}$$

where $\hat{r}$ is a unit vector in the upward direction. We calculated Ψ using SH coefficients that describe the modeled field from external sources. According to the Fukushima theorem (Fukushima, 1969), the EHIC will be the divergence-free part of the actual horizontal current field, assuming radial magnetic field lines and uniform conductance. Following for example, Laundal et al. (2016), Ψ is given by

$$\Psi = \frac{a}{\mu_0} \sum_{n,m} \frac{2n+1}{n+1} \left(\frac{a+h}{a} \right)^n P_n^m(\cos(\theta))[q_n^m \cos(m\phi) + s_n^m \sin(m\phi)] \tag{2}$$

where h is the height set at 110 km where the current is evaluated, $a = 6371.2$ km is the radius of the Earth, μ_0 is the permeability constant, ϕ is the magnetic local time converted to radians, and θ is the quasi-dipole colatitude. $P_n^m(\cos(\theta))$ are the Schmidt semi-normalized associated Legendre functions of degree n, and order m, and (q_n^m, s_n^m) are the SH coefficients describing the modeled field from external sources. We also used the Equivalent Field-Aligned Current (EFAC) as a visualization tool to track the evolution of the dayside and nightside current systems. The EFAC (Madelaire et al., 2022) is inferred from the ground assuming a uniform conductance and a ratio of 1 between Hall and Pedersen conductances. EFAC can be defined as the curl of EHIC, where EHIC is clockwise in regions with positive EFAC and anti-clockwise with negative EFAC.

To solve for the model parameters (q_n^m and s_n^m), we use iterative re-weighted least-squares with Huber weights (Madelaire et al., 2022). This reduces the influence of outliers on the final solution, which can be particularly useful in cases where the data contains a few extreme values that would otherwise skew the results (Huber, 1964). By reducing the impact of these outliers, Huber weights help ensure that the model's parameters are more representative of the data. To quantify the uncertainty in our model related to variations between events, we employed the bootstrap technique. This involves repeating the inversion process multiple times with randomly resampled substorm events. We repeated the inversion 50 times while allowing replacement using the same number of substorms. Additionally, we quantified the range of variation in the solar wind data and AL index for each substorm list using the 25th and 75th percentile of the super-posed epoch data for each list.

3. Observations

In Figures 1a and 1b, we compare the temporal evolution of the dayside dynamics between the non-substorm control group (CG) and the Newell and Gerloev (NG) substorms. The colored contours show upward (red) and downward (blue) EFACs, and the black contours show the EHIC. In Figure 1c we observe that all three IMF B_z quartiles are positive for the whole 2-hour interval, even though we applied the -45 to 20 min criterion on the IMF B_z for both CG (navy) and NG (yellow). Figure 1d shows the observed IMF B_y medians for both CG and NG, which are centered nearly around zero. In Figure 1e, we see that the AL index for the CG is almost constant during the analyzed interval of 2 hours, while a sharp change in the AL index of the NG list starts around the onset time shown in all quartiles, as well as the expected development during substorms (Baker et al., 1985; McPherron, 1995; McPherron & Manka, 1985).

Despite the IMF B_z being northward in both cases, there are notable differences between the two groups in the behavior of the dayside NBZ cells. We refer to the positive cell as the P-cell and the negative cell as the N-cell. Figure 1b shows that for the NG list, we observe an increase in the NBZ cells as well as a rise in the nightside
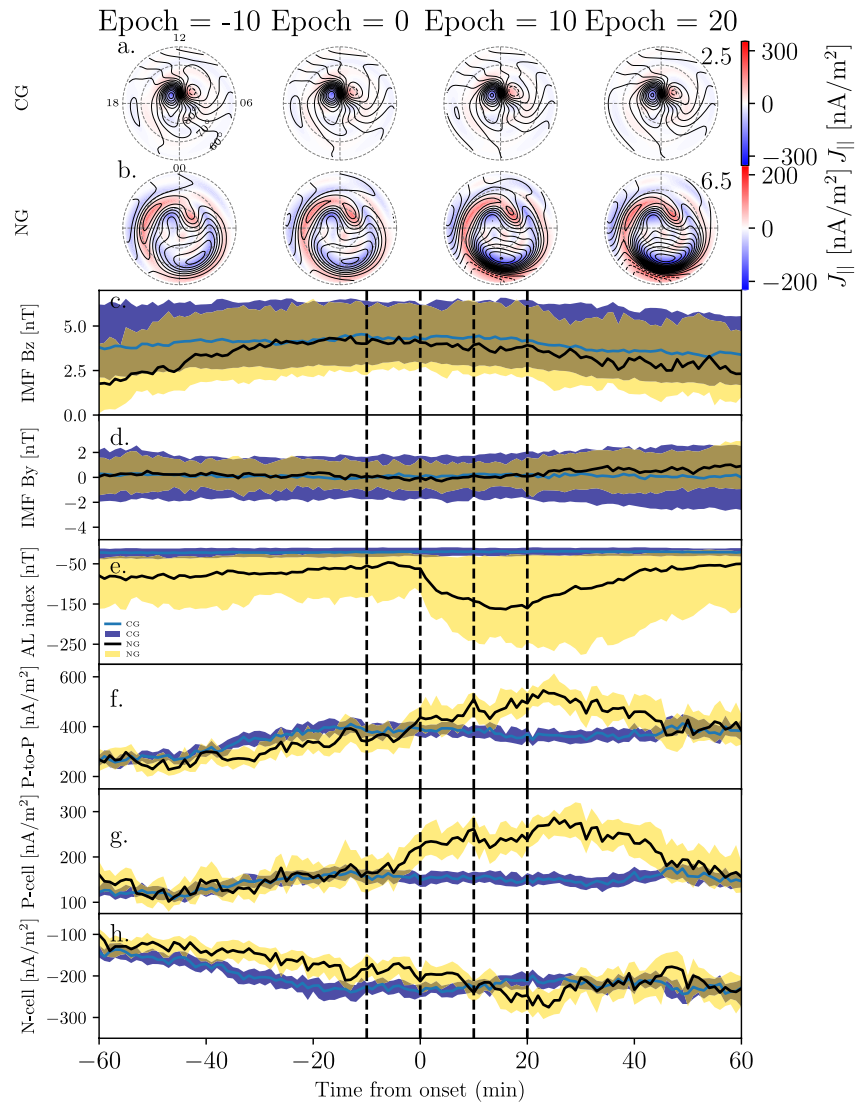
Figure 1. Comparison of the solar wind conditions and ionospheric currents between the CG and NG lists with a northward Interplanetary Magnetic Field (IMF). Panels (a) and (b) show maps of the equivalent horizontal ionospheric current (EHIC) and Equivalent Field-Aligned Current (EFAC), respectively, for the CG and NG lists. The direction of the current is clockwise in regions of downward EFAC and anti-clockwise in regions of upward EFAC. The numbers on the maps indicate the step size of Ψ in kA for CG and NG, respectively. Panels (c–h) present the IMF B_z (c), B_y (d), AL-index (e), the peak-to-peak value (f), the maximum of the P-cell (g), and the minimum of the N-cell (h) for the CG and NG lists. The blue and black lines indicate the median value for the CG and NG, respectively, and the navy and yellow shaded areas enclosed by the first and third quartiles for the CG and NG, respectively, it has been calculated through bootstrap in panels (f–h). The vertical dashed black markers correspond to the snapshots of the EHIC and EFAC maps shown in panels (a and b).

electrojet in response to the substorm onset. At epoch time −10, the NBZ cells for the NG list are weaker compared to the CG lobe cells shown in Figure 1a, and the magnitudes of the N-cell and P-cell increase as the nightside electrojets rise 10 and 20 min after the substorm onset, respectively. In order to investigate the possible influence of the solar wind velocity, density, dynamic pressure, and IMF B_x, we applied a superposed epoch analysis presented in the Supporting Information S1. None of these parameters show large variations.

In Figure 1f, we illustrate the contrasting behavior of the peak-to-peak value between the NG substorms and CG. The peak-to-peak value represents the difference between the maximum of the EFAC P-cell and the minimum of the N-cell. In the case of NG, this value increases a few minutes before substorm onset. However, there is no noticeable change for the CG. The P-cell maximum was calculated from a region between 75 and 90° latitude and 6 and 12 MLT, while the N-cell minimum was calculated from a sector between 75 and 90° latitude and 12 and 18 MLT.
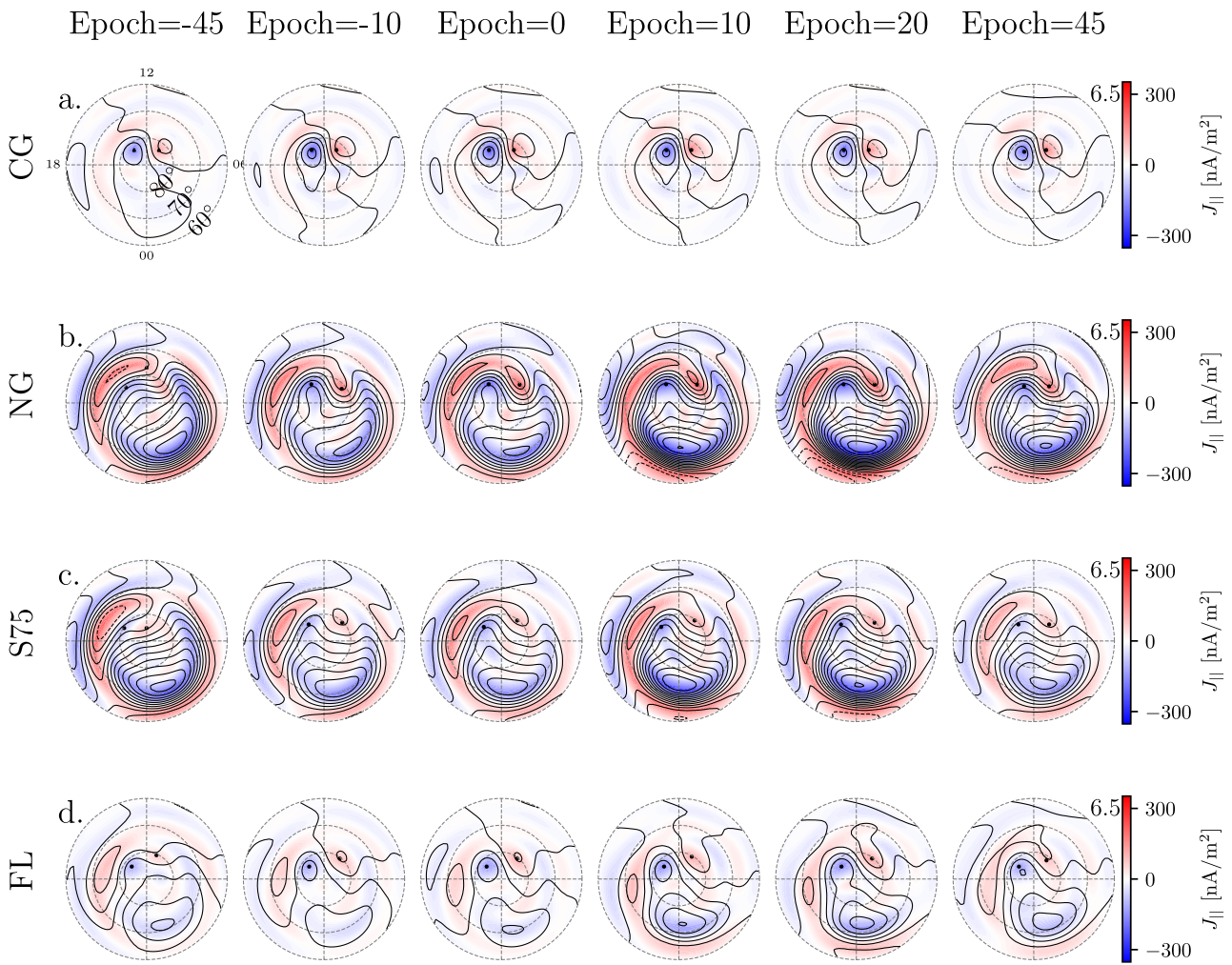
Figure 2. Maps of the Equivalent Field-Aligned Current (red/blue) and equivalent horizontal ionospheric current (black contours) for different lists under northward Interplanetary Magnetic Field conditions. Each map is oriented with magnetic noon up, midnight down, dawn on the right, and dusk on the left. Snapshots are shown at epoch times of −45, −10, 0, 10, 20, and 45 min relative to the onset time at 0. Panel (a) shows the maps for the CG, while Panels (b–d) show the results for the NG, S75, and FL lists, respectively. The numbers on the maps indicate the step size of Ψ in kA for each list.

Figure 1g shows that the P-cell magnitude for the NG list increases slightly earlier than the substorm onset, whereas, for the CG, the P-cell remains constant. Similarly, Figure 1h shows that the N-cell magnitude for the NG list increases also a few minutes prior to substorm onset, while there are no changes observed for the CG.

With the same formatting as Figures 1f–1h and 3d–3f show P-to-p, P-cell and N-cell for the CG, FL, S75, and NG lists with the lines representing the medians while the shaded areas represent the first and third quartiles.

To investigate whether the observed behavior is unique to the NG list, we analyzed two additional substorm lists (S75, FL) along with the CG. Figure 2 displays maps of the EFAC and EHIC at selected epoch times for all lists, while Figure 3 shows the temporal evolution of the IMF and geomagnetic response relative to substorm onset for each list. In Figure 2a, we observe a pronounced dayside NBZ current, while quiet levels of geomagnetic activity are observed at the nightside. All substorm lists at epoch time −45 in Figures 2b–2d show a lack of a pronounced dayside NBZ current. At epoch time −10, no noticeable change is observed for the substorm lists or the CG. However, after epoch time zero, we observe an increase in the magnitude of both the dayside P- and N-cells and the nightside EFAC and EHIC, as quantified in Figures 3c–3f. This increase is a clear response in the NG list, and a small but visible response in S75 and FL lists, although it occurs 6 min prior to onset, which we will discuss in the next section.

Figures 3d–3f shows that the magnitude of the peak-to-peak values, the maximum value of the EFAC P-cell, and the absolute value of the N-cell increase a few minutes before the onset of substorms as indicated by the thick
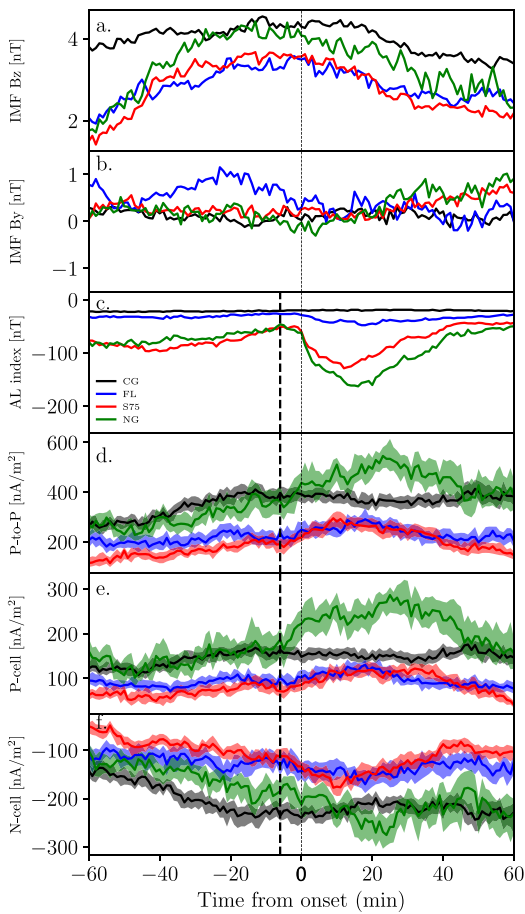
Figure 3. Comparison of solar wind conditions and ionospheric behavior for different substorm lists and a control group (CG). The panels display various parameters, with the median values represented by black (CG), blue (FL), red (S75), and green (NG) lines. The thin dashed line indicates the onset time. Panels (a and b) illustrate the solar wind Interplanetary Magnetic Field B_z and B_y conditions, respectively. Panel (c) shows the auroral lower index, while panel (d) presents the peak-to-peak values of the Equivalent Field-Aligned Current (EFAC) P- and N-cells. Panels (e and f) depict the maximum and minimum values of the EFAC P- and N-cells, respectively. The thick dashed line in panels (c–f) represents the initiation time of the dayside response, 6 min prior to the onset. The shaded areas in panels (d–f) indicate the first and third quartiles for all lists, following the same order as the median values.

dashed vertical line for all three substorm lists, while the AL index magnitude starts to increase with a little dip that increases rapidly starting on the onset. As the substorms progress, the magnitude of both the dayside and nightside current remains higher than before onset, as seen in Figures 2b–2d at epoch times 10 and 20. During the substorm recovery phase at epoch time 45, the nightside current and the dayside lobe cells gradually decay. Moreover, Figures 3d–3f demonstrates a gradual change in the dayside current for both the CG and the substorm lists from −45 to around −20, which may indicate a response to the IMF turning.

Figure 3 provides a comprehensive comparison of the solar wind and geomagnetic response to substorm onsets for both the control group and the three substorm lists. The median value of IMF B_z for the control group and the substorm lists is positive and remains constant during the two-hour interval, as shown in Figure 3a. In Figure 3b, the solar wind IMF B_y is centered around zero for the control group and two substorm lists, but it is slightly shifted toward positive values for the FL substorm list. The AL index drops significantly for the substorm lists, as seen in Figure 3c, with a sharper drop for substorms defined based on ground magnetometers than those defined based on global UV imaging (FL). The different substorm lists exhibit varying strengths of the AL index. The magnitude of the AL index is higher around epoch time 60 min prior to onset than around 45 min prior to onset when we imposed our criteria for the NG and the S75 lists which is expected during northward IMF. The AL index of the NG and S75 lists show stronger dips (below −100 nT) than the FL list. The magnitude of enhancements in NBZ currents following substorm onset also varies across the lists and is correlated with the strength of the AL index during the substorm, with NG and S75 exhibiting the clearest enhancements.

4. Discussion and Summary

We conducted a statistical analysis of ionospheric currents during substorms that occurred under northward IMF conditions. To isolate the substorm-induced dayside activity, we selected substorms with northward IMF for 45 min before onset to 20 min after onset. Since substorm onsets are defined differently based on indices from ground magnetometer measurements or based on satellite images, we studied the response for three different substorm lists using different definitions, two based on ground magnetometers (NG and S75), and one based on optical observations of the UV aurora (FL). For the S75 and NG substorm lists, we additionally restricted the clock angle to be between −45° and 45°. For the S75 list, we also restricted the minimum AL index to be less than −100 nT. Our analysis suggests that the dayside lobe cells respond to substorms, a few minutes prior to the reported onset times. The impact of nightside dynamics on dayside ionospheric currents is observed in all three different substorm lists. We found that the substorm list with the largest drop in the AL index (NG) resulted in the clearest response in the NBZ currents, while the substorm list with the weakest AL drop (FL) only indicated subtle changes in the NBZ currents associated with the onset.

There are various ways in which nightside activity could impact ionospheric electrodynamics on the dayside. One possible explanation suggested by Ohtani et al. (2021) is that FACs could respond to a remote effect of the nightside substorm current wedge, which might account for the dayside response during northward IMF substorms. However, the increase in EFAC lobe cells observed a few minutes prior to substorm onset, as seen in Figures 3c–3f from epoch −6 is inconsistent with the expected immediate response for such a remote effect, suggesting that other explanations should be explored.

Wave propagation is a fundamental process that communicates changes between the magnetosphere and the ionosphere. Different propagation times of the magnetohydrodynamic waves could be a reason for the observed response prior to substorm onset. Wave propagation through the magnetosphere can be either fast (compressive)

or slow (shear Alfvénic) waves. Magnetic reconnection events in the magnetotail generate compressive waves that can propagate along and across magnetic field lines, causing changes in plasma density and pressure. Chi et al. (2009) and Lui (2009) suggested that these fast waves can reach the ionosphere between 1.5 and 5 min after being generated in the magnetotail through the plasma sheet. However (Ferdousi & Raeder, 2016), argued that if the fast waves propagate through the lobes then the waves originating around $X \sim -10$ R$_E$ can arrive almost simultaneously to the high latitude ionosphere and can be delayed for about 20–72 s when originating around $X \sim -20$ to -30 R$_E$. Snekvik et al. (2017) observed that these waves lead to an almost immediate global response to dayside reconnection. In our analysis, we observe an enhancement in the dayside NBZ current that starts 6 min prior to substorm onset, as shown in Figures 3d–3f, which may be attributed to the arrival of compressive waves and fast plasma flows (Ohtani, 2001; Ohtani et al., 1999; Sergeev et al., 1995). The change in the magnitude of the AL index at the time indicated by the thick dashed line 6 min prior to onset as shown in Figure 3c, may also be related to the compressive waves (Machida et al., 2009; Miyashita et al., 2009).

On the other hand, slow waves are also generated by the motion of the plasma in the magnetosphere and can cause changes in the ionospheric convection pattern and are associated with the establishment of the substorm current wedge. These waves arrive at the ionosphere during the substorm expansion phase after the compressive waves, with a maximum response time of 10–20 min (G. Lu et al., 2002). By this time, the remote effect discussed earlier could partly explain the preserved elevation in the NBZ cells throughout the expansion phase, as shown in Figures 3d–3f.

The observed increase in NBZ currents during northward IMF substorms may be attributed to changes in the lobe reconnection rate, which are influenced by variations in the magnetopause topology. The IMF B_z component strongly affects the degree of flaring of the magnetopause (Shue et al., 1997). When new magnetic flux is added to the lobes, the tail of the magnetosphere extends further. However, during northward IMF conditions, the magnetosphere takes on a more blunt shape (Shue et al. (1997); J. Y. Lu et al (2011).). Lobe reconnection occurs just tailward of the cusp, where the local geometry differs between the flaring and blunt-shaped magnetosphere. The precise impact of these geometrical changes on the lobe reconnection rate is still unclear. However, it is known that strong lobe reconnection typically occurs during northward IMF conditions. Before a substorm, the magnetotail lobes need to be loaded, resulting in outward flaring of the magnetotail during northward IMF substorms compared to the control group. The substorm process leads to changes in the tail state (Eather et al., 1979), possibly causing a more blunt-shaped magnetopause as magnetic flux becomes closed. Therefore, the observed changes in NBZ currents shown in Figure 2b–2d may reflect variations in the lobe reconnection rate associated with topological changes of the magnetosphere during the substorm.

In summary, we analyzed three substorm lists and found that during northward IMF, the dayside ionospheric currents, as observed with ground magnetometers, respond to substorm activity by increasing the magnitude of the NBZ cells. We found that substorm lists with higher AL index exhibit a higher response in NBZ cells, as shown in Figures 2b–2d and 3c–3f. Interestingly, the NBZ cell response begins a few minutes before substorm onset. We have discussed three possible effects that could account for the observed dayside response to substorms.

- The remote nightside current and the establishment of the substorm current wedge may explain the increase observed in the dayside NBZ cells after onset. However, this factor alone is insufficient to capture the impact prior to substorm onset.
- Compressive and shear Alfvénic waves are mechanisms for communicating between the magnetosphere and the ionosphere. Initially fast mode waves (compressive) could reach the ionosphere before the establishment of a substorm current wedge, and be responsible for the observed dayside enhancement prior to the substorm onset. This is followed by shear Alfvénic waves sustaining the increase during the substorm expansion phase.
- Changes in flaring angle could enhance the lobe reconnection efficiency, maintaining the elevated NBZ cells throughout the substorm.

Data Availability Statement

Magnetometer data can be downloaded directly from https://supermag.jhuapl.edu/mag/ where you need to specify the year to download. Solar wind data (OMNI) can be downloaded from https://cdaweb.gsfc.nasa.gov/sp_phys/data/omni/hro_1min/. Gjerloev and Newell, SOPHIE75, Frey and Liou lists could be downloaded from https://supermag.jhuapl.edu/substorms/ The substorm lists after applying our selection criteria can be downloaded from: https://doi.org/10.5281/zenodo.7990528.

References

Baker, D. N., Fritz, T. A., McPherron, R. L., Fairfield, D. H., Kamide, Y., & Baumjohann, W. (1985). Magnetotail energy storage and release during the CDAW 6 substorm analysis intervals. *Journal of Geophysical Research*, *90*(A2), 1205–1216. https://doi.org/10.1029/JA090iA02p01205

Chi, P. J., Russell, C. T., & Ohtani, S. (2009). Substorm onset timing via traveltime magnetoseismology. *Geophysical Research Letters*, *36*(8), L08107. https://doi.org/10.1029/2008GL036574

Cowley, S. W. H., & Lockwood, M. (1992). Excitation and decay of solar-wind driven flows in the magnetosphere-ionosphere system. *Annales Geophysicae*, *10*, 103–115. Retrieved from https://centaur.reading.ac.uk/38840/

Eather, R., Mende, S., & Weber, E. (1979). Dayside aurora and relevance to substorm current systems and dayside merging. *Journal of Geophysical Research*, *84*(A7), 3339–3359. https://doi.org/10.1029/JA084iA07p03339

Ferdousi, B., & Raeder, J. (2016). Signal propagation time from the magnetotail to the ionosphere: Openggcm simulation. *Journal of Geophysical Research*, *121*(7), 6549–6561. https://doi.org/10.1002/2016JA022445

Forsyth, C., Rae, I. J., Coxon, J. C., Freeman, M. P., Jackman, C. M., Gjerloev, J., & Fazakerley, A. N. (2015). A new technique for determining substorm onsets and phases from indices of the electrojet (Sophie). *Journal of Geophysical Research: Space Physics*, *120*(12), 10592–10606. https://doi.org/10.1002/2015JA021343

Freeman, M. P., Farrugia, C. J., Burlaga, L. F., Hairston, M. R., Greenspan, M. E., Ruohoniemi, J. M., & Lepping, R. P. (1993). The interaction of a magnetic cloud with the Earth: Ionospheric convection in the northern and southern hemispheres for a wide range of quasi-steady interplanetary magnetic field conditions. *Journal of Geophysical Research*, *98*(A5), 7633–7655. https://doi.org/10.1029/92JA02350

Frey, H. U., Mende, S. B., Angelopoulos, V., & Donovan, E. F. (2004). Substorm onset observations by IMAGE-FUV. *Journal of Geophysical Research*, *109*(A10), 2. https://doi.org/10.1029/2004JA010607

Fukushima, N. (1969). Equivalence in ground geomagnetic effect of chapman–vestine's and Birkeland–Alfven's electric current-systems for polar magnetic storms. *Report of Ionosphere and Space Research in Japan*, *23*, 219–227. Retrieved from https://www.osti.gov/biblio/4755464

Gjerloev, J. W. (2012). The SuperMAG data processing technique. *Journal of Geophysical Research*, *117*(9), 1–19. https://doi.org/10.1029/2012JA017683

Grocott, A., Cowley, S. W. H., Sigwarth, J. B., Watermann, J. F., & Yeoman, T. K. (2002). Excitation of twin-vortex flow in the nightside high-latitude ionosphere during an isolated substorm. *Annales Geophysicae*, *20*(10), 1577–1601. https://doi.org/10.5194/angeo-20-1577-2002

Grocott, A., Laurens, H. J., & Wild, J. A. (2017). Nightside ionospheric convection asymmetries during the early substorm expansion phase: Relationship to onset local time. *Geophysical Research Letters*, *44*(23), 11696–11705. https://doi.org/10.1002/2017GL075763

Huber, P. J. (1964). Robust estimation of a location parameter. *The Annals of Mathematical Statistics*, *35*(1), 73–101. https://doi.org/10.1214/aoms/1177703732

Iijima, T. (1984). Field-aligned currents during northward IMF. In *Magnetospheric currents* (pp. 115–122). American Geophysical Union (AGU). https://doi.org/10.1029/GM028p0115

Laundal, K. M., Finlay, C. C., Olsen, N., & Reistad, J. P. (2018). Solar wind and seasonal influence on ionospheric currents from swarm and champ measurements. *Journal of Geophysical Research: Space Physics*, *123*(5), 4402–4429. https://doi.org/10.1029/2018JA025387

Laundal, K. M., Gjerloev, J. W., Østgaard, N., Reistad, J. P., Haaland, S., Snekvik, K., et al. (2016). The impact of sunlight on high-latitude equivalent currents. *Journal of Geophysical Research: Space Physics*, *121*(3), 2715–2726. https://doi.org/10.1002/2015JA022236

Lee, D., Choi, K., Ohtani, S., Lee, J. H., Kim, K. C., Park, K. S., & Kim, K. H. (2010). Can intense substorms occur under northward IMF conditions? *Journal of Geophysical Research*, *115*(A1), A01211. https://doi.org/10.1029/2009JA014480

Lee, D., Ohtani, S., & Lee, J. H. (2010). On the poleward boundary of the nightside auroral oval under northward interplanetary magnetic field conditions. *Journal of Geophysical Research*, *115*(A8), A08204. https://doi.org/10.1029/2009JA014906

Liou, K. (2010). Polar Ultraviolet Imager observation of auroral breakup. *Journal of Geophysical Research*, *115*(12), 1–7. https://doi.org/10.1029/2010JA015578

Lu, G., Holzer, T. E., Lummerzheim, D., Ruohoniemi, J. M., Stauning, P., Troshichev, O., et al. (2002). Ionospheric response to the interplanetary magnetic field southward turning: Fast onset and slow reconfiguration. *Journal of Geophysical Research*, *107*(A8), SIA2-1–SIA2-9. https://doi.org/10.1029/2001JA000324

Lu, J. Y., Liu, Z.-Q., Kabin, K., Zhao, M. X., Liu, D. D., Zhou, Q., & Xiao, Y. (2011). Three dimensional shape of the magnetopause: Global MHD results. *Journal of Geophysical Research*, *116*(A9), A09237. https://doi.org/10.1029/2010JA016418

Lui, A. T. Y. (2009). Comment on "tail reconnection triggering substorm onset". *Science*, *324*(5933), 1391. https://doi.org/10.1126/science.1167726

Machida, S., Miyashita, Y., Ieda, A., Nosé, M., Nagata, D., Liou, K., et al. (2009). Statistical visualization of the Earth's magnetotail based on geotail data and the implied substorm model. *Annales Geophysicae*, *27*(3), 1035–1046. https://doi.org/10.5194/angeo-27-1035-2009

Madelaire, M., Laundal, K. M., Reistad, J. P., Hatch, S. M., & Ohma, A. (2022). Transient high latitude geomagnetic response to rapid increases in solar wind dynamic pressure. *Frontiers in Astronomy and Space Sciences*, *9*. https://doi.org/10.3389/fspas.2022.953954

McPherron, R. L. (1995). 13 magnetospheric dynamics. In *Chapter 13 introduction to space physics*.

McPherron, R. L., & Manka, R. H. (1985). Dynamics of the 1054ut march 22,1979, substorm event: CDAW 6. *Journal of Geophysical Research*, *90*(A2), 1175–1190. https://doi.org/10.1029/JA090iA02p01175

Milan, S. E. (2015). Sun et lumière: Solar wind-magnetosphere coupling as deduced from ionospheric flows and polar auroras.

Milan, S. E., Gosling, J. S., & Hubert, B. (2012). Relationship between interplanetary parameters and the magnetopause reconnection rate quantified from observations of the expanding polar cap. *Journal of Geophysical Research*, *117*(A3), A03226. https://doi.org/10.1029/2011JA017082

Milan, S. E., Grocott, A., & Hubert, B. (2010). A superposed epoch analysis of auroral evolution during substorms: Local time of onset region. *Journal of Geophysical Research*, *115*(A5), A00I04. https://doi.org/10.1029/2010JA015663

Miyashita, Y., Kamide, Y., Liou, K., Wu, C.-C., Ieda, A., Nishitani, N., et al. (2011). Successive substorm expansions during a period of prolonged northward interplanetary magnetic field. *Journal of Geophysical Research*, *116*(A9), A09221. https://doi.org/10.1029/2011JA016719

Miyashita, Y., Machida, S., Kamide, Y., Nagata, D., Liou, K., Fujimoto, M., et al. (2009). A state-of-the-art picture of substorm-associated evolution of the near-Earth magnetotail obtained from superposed epoch analysis. *Journal of Geophysical Research*, *114*(A1), A01211. https://doi.org/10.1029/2008JA013225

Newell, P. T., & Gjerloev, J. W. (2011). Substorm and magnetosphere characteristic scales inferred from the supermag auroral electrojet indices. *Journal of Geophysical Research*, *116*(A12), A12232. https://doi.org/10.1029/2011JA016936

Ohma, A., Reistad, J. P., & Hatch, S. M. (2021). Modulation of magnetospheric substorm frequency: Dipole tilt and IMF by effects. *Journal of Geophysical Research: Space Physics*, *126*(3), e2020JA028856. https://doi.org/10.1029/2020JA028856

Ohtani, S. (2001). Substorm trigger processes in the magnetotail: Recent observations and outstanding issues. *Space Science Reviews*, *95*(1–2), 347–359. https://doi.org/10.1023/a:1005231122496

Ohtani, S., Creutzberg, F., Mukai, T., Singer, H., Lui, A. T. Y., Nakamura, M., et al. (1999). Substorm onset timing: The December 31, 1995, event. *Journal of Geophysical Research*, *104*(A10), 22713–22727. https://doi.org/10.1029/1999JA900209

Ohtani, S., Imajo, S., Nakamizo, A., & Gjerloev, J. W. (2021). Globally correlated ground magnetic disturbances during substorms. *Journal of Geophysical Research: Space Physics*, *126*(4), e2020JA028599. https://doi.org/10.1029/2020JA028599

Peng, Z., Wang, C., Yang, Y. F., Hu, H. L. Y. Q., & Du, J. (2013). Substorms under northward interplanetary magnetic field: Statistical study. *Journal of Geophysical Research: Space Physics*, *118*(1), 364–374. https://doi.org/10.1029/2012JA018065

Provan, G., Lester, M., Mende, S. B., & Milan, S. E. (2004). Statistical study of high-latitude plasma flow during magnetospheric substorms. *Annales Geophysicae*, *22*(10), 3607–3624. https://doi.org/10.5194/angeo-22-3607-2004

Reistad, J. P., Laundal, K. M., Østgaard, N., Ohma, A., Thomas, E. G., Haaland, S., et al. (2019). Separation and quantification of ionospheric convection sources: 2. The dipole tilt angle influence on reverse convection cells during northward IMF. *Journal of Geophysical Research: Space Physics*, *124*(7), 6182–6194. https://doi.org/10.1029/2019JA026641

Senior, C., Cerisier, J.-C., Rich, F., Lester, M., & Parks, G. K. (2002). Strong sunward propagating flow bursts in the night sector during quiet solar wind conditions: Superdarn and satellite observations. *Annales Geophysicae*, *20*(6), 771–779. https://doi.org/10.5194/angeo-20-771-2002

Sergeev, V. A., Angelopoulos, V., Mitchell, D. G., & Russell, C. T. (1995). In situ observations of magnetotail reconnection prior to the onset of a small substorm. *Journal of Geophysical Research*, *100*(A10), 19121–19133. https://doi.org/10.1029/95JA01471

Shue, J.-H., Chao, J. K., Fu, H. C., Russell, C. T., Song, P., Khurana, K. K., & Singer, H. J. (1997). A new functional form to study the solar wind control of the magnetopause size and shape. *Journal of Geophysical Research*, *102*(A5), 9497–9511. https://doi.org/10.1029/97JA00196

Snekvik, K., Østgaard, N., Tenfjord, P., Reistad, J. P., Laundal, K. M., Milan, S. E., & Haaland, S. E. (2017). Dayside and nightside magnetic field responses at 780 km altitude to dayside reconnection. *Journal of Geophysical Research: Space Physics*, *122*(2), 1670–1689. https://doi.org/10.1002/2016JA023177

Tenfjord, P., Østgaard, N., Strangeway, R., Haaland, S., Snekvik, K., Laundal, K. M., et al. (2017). Magnetospheric response and reconfiguration times following IMF by reversals. *Journal of Geophysical Research: Space Physics*, *122*(1), 417–431. https://doi.org/10.1002/2016JA023018

Weimer, D. R. (2005). Improved ionospheric electrodynamic models and application to calculating joule heating rates. *Journal of Geophysical Research*, *110*(A5), A05306. https://doi.org/10.1029/2004JA010884

Yu, Y., & Ridley, A. J. (2009). Response of the magnetosphere-ionosphere system to a sudden southward turning of interplanetary magnetic field. *Journal of Geophysical Research*, *114*(A3), A03216. https://doi.org/10.1029/2008JA013292